Effects of Casing Shape on the Performance of a Small-sized Centrifugal Compressor

D.-W. Kim, H.-S. Kim, Youn J. Kim†

School of Mechanical Engineering, SungKyunKwan University, Suwon 440-746, Korea

Key words: Centrifugal compressor, Volute casing, Circular casing, Pressure recovery coefficient, Loss coefficient, Archimedes spiral

ABSTRACT: The effects of casing shapes on the performance and the interaction between an impeller and a casing in a small-sized centrifugal compressor are investigated. Especially, numerical analyses are conducted for the centrifugal compressor with both a circular casing and a volute one. The optimum design for each element (i.e., impeller, diffuser and casing) is important to develop an efficient and compact compressor using alternative refrigerant as working fluids. Typical rotating speed of the compressor is in the range of 40,000~45,000 rpm. The impeller has backswept blades due to tip clearance and a vane diffuser has wedge type. In order to predict the flow pattern inside an entire impeller, vaneless diffuser and casing, calculations with multiple frames of reference method between the rotating and stationery parts of the domain are carried out. For computations of compressible turbulent flow fields, the continuity and time-averaged Navier-Stokes equations are employed. To evaluate the performance of two types of casings, the static pressure recovery and loss coefficients are obtained for various flow rates. Also, static pressure distributions around casings are studied for different casing shapes, which are very important to predict the distribution of radial load. The static pressure around the casing and pressure difference between the inlet and outlet of the compressor are measured for the circular casing.

Nomenclature

c_p : pressure recovery
R : gas constant; rothalpy
T : absolute temperature
u_i : velocity (i=1, 2, 3)
u_i' : RMS perturbation velocity
w : loss coefficient

Greek symbols

δ_{ij} : Kronecker delta fuction
ε_{ijk} : permutation tensor
μ : absolute fluid viscosity

Subscripts

0 : inlet of centrifugal compressor
1, 2 : inlet/outlet of impeller
3, 4 : inlet/outlet of diffuser
5 : inside of casing
6 : outlet of centrifugal compressor
d : design point

† Corresponding author
Tel.: +82-31-290-7448; fax: +82-31-290-5849
E-mail address: kimyj@me.skku.ac.kr

1. Introduction

A centrifugal compressor is expected to replace a scroll compressor as the component of

an air conditioner, because it has lots of merits, such as low noise, non-lubrication, and high performance. The static pressure difference of the centrifugal compressor with a volute casing is generally increased more than that with circular one. However, the defect of a gas bearing, which is typically equipped in high rotating speed of the centrifugal compressor, will be increased in the volute casing and the operation of the centrifugal compressor could be unstable due to radial force on the bearing. Furthermore, small mistakes on the design of a volute casing will be resulted in more swirl and loss and these lead to lose the kinetic energy added by the impeller. Therefore, the casing design is one of the significant processes for improving the performance of a centrifugal compressor.

Majidi[1] analyzed numerically the three-dimensional viscous flow fields for the concentric and volute casings. Especially, he reported that the swirl in the casing seriously affects on the performance of the compressor.

Lorett et al.[2] showed that the non-uniform distribution of velocity and pressure at the impeller exit and the cyclic variation of flow in the impeller channels influenced on flow field in the volute casing and compared the numerical result with empirical one. They reported that the boundary condition of irregular inward flow to the volute casing should be considered for better understanding flow fields, because unstable and cyclic flows practically occur at the exit of the impeller.

Croba and Kueny[3] analyzed the characteristics of velocity and pressure occurred by periodic discharge of working fluid in the two-dimensional shape of the volute casing by numerical and experimental methods. To treat the interface between the impeller and the volute, they used the multi-domain overlapping grid technique.

Hillewaert and Braembussche[4] investigated the interaction of the centrifugal compressor with unsteady analysis on the impeller and with steady analysis on the volute casing. They also carried out the experiment to prove the numerical results.

Ayder et al.[5] elucidated that the kinetic energy irreversibly reduced and the irregular pressure distribution occurred along the volute passage at the off-design point. These might be resulted in unsteady operation, vibration, and reduction of efficiency.

Braembussche et al.[6] developed the analytical equations to predict the unsteady flow occurred at the impeller and the diffuser, and proved these by means of experiment.

In this study, we have investigated the effects of casing shapes on performance and interaction between the impeller and the casing in the small-sized centrifugal compressor by numerical and experimental methods.

2. Numerical analysis

2.1 Description of modeled centrifugal compressor

The domain of numerical analysis consists of the impeller, the vaneless diffuser and the casing (see Fig. 1). Table 1 shows operating conditions. The circular casing with a rectangular cross section and the volute casing with ellip-

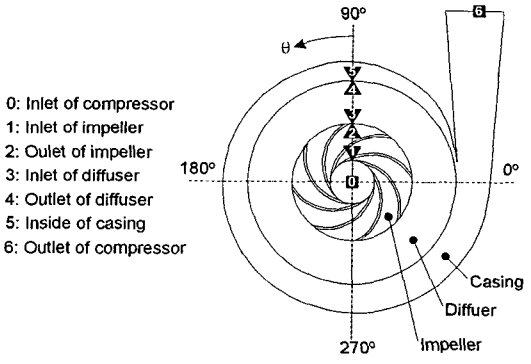

Fig. 1 Geometry of the modeled centrifugal compressor.

Table 1 Specifications and operating conditions of the modeled centrifugal compressor

Diameter of impeller	52 mm
Height of impeller exit	1.9 mm
Diameter of diffuser	90 mm
Rotating speed	45,000 rpm
Design flow rate	82 g/s

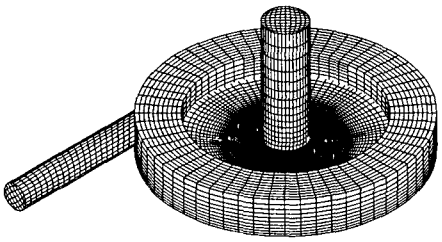

(a) Circular casing

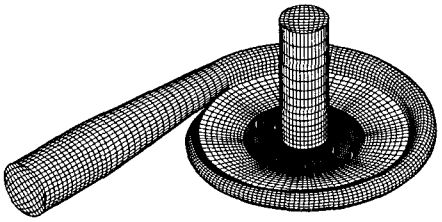

(b) Volute casing

Fig. 2 Schematic of the grid systems of casings.

tic one are respectively used to compare shape effects on the performance and interaction between the impeller and casing.

A volute spiral is designed by one curve to keep constant throughput velocity at all sections of the volute.[7] That curve is named Archimedes spiral. The numerical domain with body-fitted coordinates made by the staggered grid system with 68,000 cells (see Fig. 2). Grid system was determined to be the practical after running test cases with various numbers of nodes.

2.2 Governing equations

The steady, turbulence, viscous, and time averaged governing equations (Reynolds equation) by tensor notation can be expressed as follows:

$$\frac{\partial}{\partial x_j}(\rho u_j) = 0 \tag{1}$$

$$\frac{\partial}{\partial x_j}(\rho u_j u_i - \tau_{ij}) = -\frac{\partial p}{\partial x_i} + s_i \tag{2}$$

$$\frac{\partial}{\partial x_j}(\rho u_j R - F_{h,j} - u_i \tau_{ij}) = s_i u_i \tag{3}$$

where τ_{ij} (friction term), $F_{h,j}$ (diffusion term), s_i (rotating force), and R (rothalpy) are written as follows:

$$\tau_{ij} = \mu\left(\frac{\partial u_i}{\partial x_j} + \frac{\partial u_j}{\partial x_i}\right) - \frac{2}{3}\mu\frac{\partial u_k}{\partial x_k}\delta_{ij} - \rho\overline{u_i' u_j'} \tag{4}$$

$$F_{h,j} = \kappa\frac{\partial T}{\partial x_j} - \rho\overline{u_j' h'} \tag{5}$$

$$s_i = -2\rho\varepsilon_{ijk}\omega_j u_k - \rho(\omega_m \omega_m x_i - \omega_n \omega_n x_i) \tag{6}$$

$$R = h + \frac{(\vec{u})^2}{2} - \frac{(\vec{\omega}\times\vec{r})^2}{2} \tag{7}$$

Above non-linear governing equations were discretized by means of FVM (finite volume method). Also we applied hybrid scheme for convective and diffusion terms. SIMPLE (semi-implicit method for pressure-linked equation) algorithm was used to combine the continuity equation with the momentum equation. The standard $\kappa-\varepsilon$ model was used as the turbulence model.

A subroutine program to calculate the following state and specific heat equations was coded, because RC-318 as working fluid has the different characteristics from an ideal gas.[8]

$$p = \frac{R_g T}{\nu - b} + \sum_{i=2}^{5}\frac{1}{(\nu-b)^i}\left(A_i + B_i T + C_i e^{-\kappa T/T_c}\right) \tag{8}$$

$$C_p = \sum_{i=1}^{4} G_i T^{i-1} - R_g \tag{9}$$

Table 2 Constants of the state and specific heat equations in (8) and (9)

T_c	388.48 K	B_4	0.0
x	5.0	B_5	9.73125201e−12
b	3.753e−4	C_2	−7.66941499e+2
R	41.5628	C_3	1.11357942
A_2	−5.09125078e+1	C_4	0.0
A_3	4.44191073e−4	C_5	−2.51636825e−7
A_4	−2.57248397e−5	G_1	9.427759077e+1
A_5	3.98047697e−9	G_2	2.787714064
B_2	4.76339868e−2	G_3	−2.236127054e−3
B_3	−2.07196888e−5	G_4	5.256534892e−7

where A, B, C, x and G are constants (see Table 2). In order to elucidate the performance of the casing, the static pressure recovery coefficient and the loss coefficient are introduced as follows:

$$c_p = \frac{P_6 - P_4}{P_4^o - P_4} \tag{10}$$

$$w = \frac{P_4^o - P_6^o}{P_4^o - P_4} \tag{11}$$

in which the numbered subscripts are denoted in Figs. 1 and 3.

2.3 Boundary conditions

Flow variables should be given on the inlet boundary, and turbulence kinetic energy (κ) and turbulence kinetic energy dissipation (ε) should be calculated in the numerical domain. Because the isotropic of turbulence is assumed in $\kappa-\varepsilon$ turbulence model, turbulence intensity (I) and turbulence kinetic energy can be written as follows:

$$I = \frac{u'}{U} \times 100 \tag{12}$$

$$k = 1.5\left(I\frac{U}{100}\right)^2 \tag{13}$$

$$\varepsilon = C_\mu \frac{k^{3/2}}{l} \tag{14}$$

where u' is the fluctuation of velocity, U is the average inlet velocity, C_μ is 0.09, respectively. The characteristic length is defined by the 1/100 times height of the inlet of the impeller. No-slip condition is used on the wall boundary and it is presumed that there is no mass flux at wall. In order to reduce cells, the wall functions were used. Therefore, first cell from wall is located in which the value of non-dimensional length ($y^+ = yu_\tau/\nu$) is 30~300. Because we can hardly know flow variables on the outlet boundary, Neumann condition that has zero gradient for all flow variables along streamlines are applied.

2.4 Experimental apparatus

The schematic diagram of the experimental apparatus is shown in Fig. 3. Refrigerant in gas is compressed by the centrifugal compressor and passed through a condenser without fully saturated and then it is enlarged right after a condenser without an evaporator.

In order to control temperature at the inlet and outlet, SSR (solid state relay) handles a fan that is installed in the condenser. The centrifugal compressor with the gas bearing due to high speed is vertically mounted. Motor speed is set by changing the frequency of electrical source and flow rate is measured by orifice

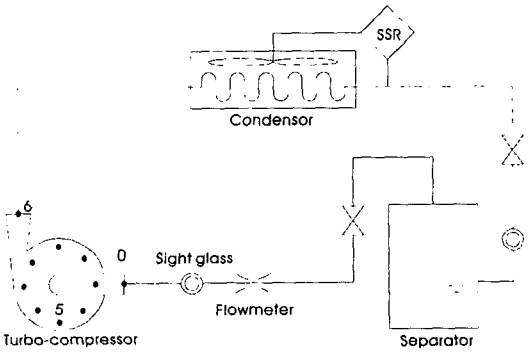

Fig. 3 Schematic diagram of experimental apparatus.

flowmeter on the suction pipe. Data were stored by the data acquisition board (Daqview, I/O Tech). Thermocouples (T-type, OMEGA) and pressure transducer (DSA 3017, Scannivalve, accuracy 0.05% at 5 to 500 psi, 200 sample/sec) are used to measure temperature and pressure.

In order to measure static pressure around the casing, we machined eight holes every 45° from 0° to 360°.

The prototype impeller, the diffuser and the circular and the volute casings are chosen to measure the performance and static pressure. To begin with, a motor speed (rpm) keeps constant and the opening of a flow control valve is controlled to vary flow rate, and measured the flow rate and the inlet and outlet pressures. Also, we kept constantly outlet pressure, flow rate and temperature.

3. Results and discussion

In order to improve the performance and the safety of the centrifugal compressor during operation, the interaction between the impeller and casing is predicted by numerical and experimental analyses.

For the case of the circular casing that may have little effect on the interaction, performance that means pressure difference between the inlet and the outlet of the centrifugal compressor (P_{S6}-P_{S0}) normalized by inlet pressure (P_{S0}) is smaller than that of the volute casing at all flow rates (see Fig. 4).

For the case of the volute casing, it may have the larger flow rate than the circular casing because normalized pressure difference increases as the flow rate goes up. The volute casing comparing with the circular one extends the range of the flow rate.

Results of numerical analysis show that the performance of the volute casing has greater than that of the circular one at all flow rates. To prove numerical results, the experiment with the circular casing was carried out. As shown in Fig. 4, comparison between numerical and experimental results shows a good agreement. In more detail, experimental results show some larger due to the difference of the shape from machining tolerance and grid simplification.

Static pressure recovery coefficient and loss coefficient at various flow rates are plotted in Figs. 5 and 6. Static pressure recovery coeffi-

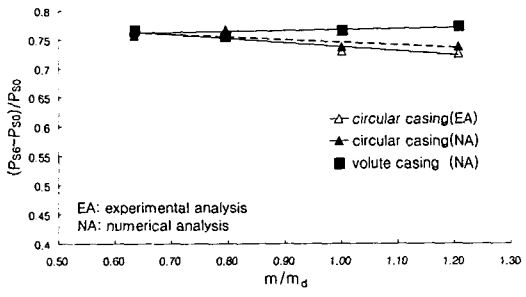

Fig. 4 Overall performance with various flow rates (NA: Numerical analysis, EA: Experimental analysis).

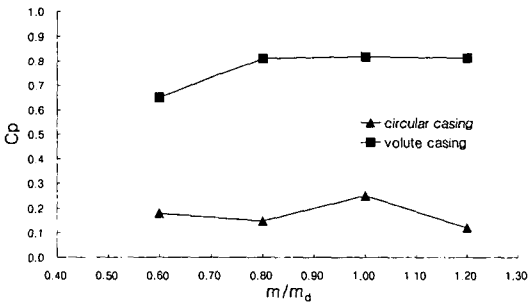

Fig. 5 Static pressure recovery coefficient with various flow rates.

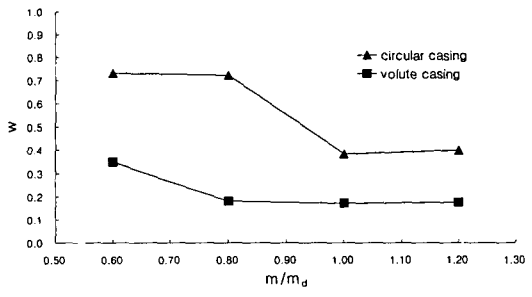

Fig. 6 Loss coefficient with various flow rates.

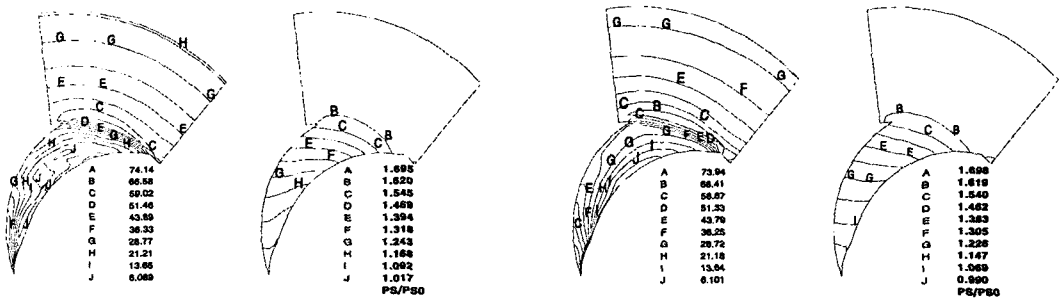

(a) Circular casing (b) Volute casing

Fig. 7 Velocity and static pressure distributions in impeller and diffuser (unit: m/s, Pa).

cient is defined as the ratio of static pressure rise in the casing and dynamic pressure at the inlet of the casing as Eq. (10).

Loss coefficient is also defined as the ratio of total pressure rise in casings and dynamic pressure at the inlet of the casing as Eq. (11). Because the dynamic pressure converted to the static pressure in the casing, two coefficients are important values to evaluate the casing performance.

For the case of the volute casing, static pressure coefficient increases and loss coefficient decreases as the flow rate increases. Also, the volute casing has better performance than the circular one, since it has high pressure-recovery coefficient and low loss coefficient.

Fig. 7 shows the velocity and static pressure distribution for two casings with the same impeller and diffuser. Because of the interaction between the impeller and casing, the same impeller channel in the different casing shows different flow pattern. In addition, there are stall regions near the pressure surface (the right side of the impeller channel) of this back swept impeller blade in both casings. In the circular casing, the stall region as a flow blockage occurred on a half of the width of the impeller channel. And this region occurred on one-third in the volute one. These stall regions, low kinetic energy zones, will be resulted in loss.

These phenomena could be also shown in pressure distribution. In the distribution of static pressure in Fig. 7 (a), isobaric lines indicate different gradients near the mid-length of the impeller channel width, which shows the difference of reversed pressure gradient.

As shown in Fig. 7 (b), gradient change for the volute casing moves close to the pressure surface. The velocity and pressure of the working fluid increases through the impeller channel due to energy added by the rotating impeller. And, at the impeller exit, velocity reached up to 66 m/s and Mach number is 0.55. This high-speed fluid decreases to 25 m/s at the casing inlet. The major function of the casing is the collection of the working fluid to the casing exit and the transportation between the dynamic pressure and static pressure. In the circular casing, most of flow results from radial velocity at the diffuser exit, but flow consists

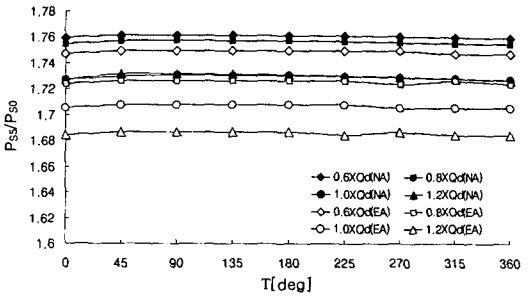

Fig. 8 Circumferential static pressure distribution with four operation points (circular casing).

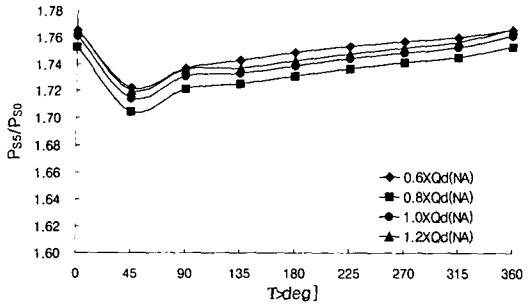

Fig. 9 Circumferential static pressure distribution with four operation points (volute casing).

of both radial and tangential velocity components in the volute one. These flow patterns in casings influence apparently the distribution of the static pressure.

The static pressure distributions around the casings are shown in Figs. 8~10. Static pressure around the casing normalized by inlet pressure shows similar values in Fig. 8. In the circular casing, the highest static pressure occurred from 45° to 95° of circumferential direction, and due to large radial velocity of main flow, static pressure rises along the radial direction, drawing the concentric circle (see Fig. 10 (a)). The pressure distribution in the experimental result is similar to numerical one. Although the distribution trends are almost similar, there are some differences between the numerical and experimental results.

As shown in Fig. 9, the static pressure in the volute casing rises from the volute tongue to the exit nozzle of the casing, which represents the characteristics of flow pattern as the general diffuser. In aspect of pressure difference, pressure goes up along both the radial and tangential directions against the case in the circular casing (see Fig. 10 (b)). The angle of lowest pressure occurred at 45° in comparison with the volute casing.

Static pressure distributions around both the circular and volute casings show respectively typical characteristics at design and lower flow rates.

4. Conclusions

We have studied the effects of casing shapes on the performance of the small-sized centrifugal compressor for both circular and volute casings, and concluded as follows:

(1) In analyses on performance of the casing of the centrifugal compressor, the volute casing shows better performance comparing with the circular one.

(2) In the same impeller channel, the significant difference values of velocity and pressure occurred due to interaction between the casing and impeller. The two-zone having low and high momentums are observed in the impeller. In the case of the volute casing, the small stall region that may cause the loss was made.

(3) As analyzing pressure distribution around

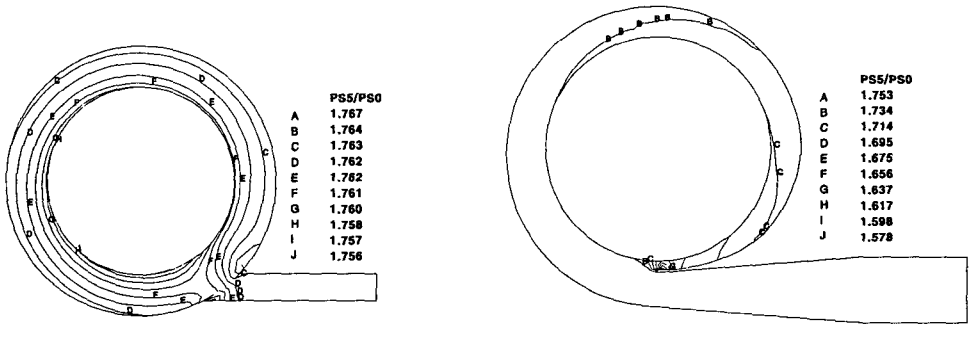

(a) Circular casing (b) Volute casing

Fig. 10 Circumferential static pressure distribution at design point (unit: Pa).

the casing, the centrifugal compressor with circular casing operated near design point and that with the volute one ran at the off-design point, the left side of the design point.

Acknowledgments

The authors are grateful for the financial support provided by the Korea Ministry of Education through the Brain Korea 21 project.

References

1. Majidi, K., 1998, Numerical calculation of secondary flow in pump volute and circular casings using 3D viscous flow techniques, Proceedings of the 7th International Symposium on Transport Phenomena and Dynamics of Rotating Machinery, Vol. C, pp. 1459-1469.
2. Lorett, J. A. and Gopalakrishnan, S., 1986, Interaction between impeller and volute of pumps at off-design conditions, ASME J. of Fluids Engineering, Vol. 108, No. 1, pp. 12-18.
3. Croba, D. and Kueny, J. L., 1996, Numerical calculation of 2D, unsteady flow in centrifugal pumps: Impeller and volute interaction, Int'l J. for Numerical in Fluids, Vol. 22, pp. 467-481.
4. Hillewaert, K. and Van den Braembussche, R. A., 1999, Numerical simulation of impeller-volute interaction in centrifugal compressor, J. of Turbomachinery, Vol. 121, pp. 603-608.
5. Ayder, E., Braembussche, R. A. and Brasz, J. J., 1993, Experimental and theoretical analysis of the flow in a centrifugal compressor volute, ASME J. of Turbomachinery, Vol. 115, pp. 582-589.
6. Van den Braembussche, R. A., Ayder, E. and Keiper, R, 1999, Improved model for the design and analysis of centrifugal compressor volutes, J. of Turbomachinery, Vol. 121, pp. 619-625.
7. Stepanoff, A. J., 1957, Centrifugal and Axial Flow Pumps, John Wiley & Sons, New York.
8. Reynolds, W. T., 1979, Thermodynamic Property in SI, Stanford University Press, Stanford.
9. Japikse, D. and Baines, N. C., Introduction to turbomachinery, J. Concepts ETI, Inc and Oxford University Press, New York.